Journal of Mines, Metals and Fuels, *71(12C) : 483-493; 2023. DOI: 10.18311/jmmf/2023/47320*

Print ISSN : 0022-2755

Journal of Mines, Metals and Fuels

Contents available at: *www.informaticsjournals.com/index.php/jmmf*

Exploring Boronic Acid Derivative through their Photophysical Properties, Quantum Chemical Computations and Molecular Docking

P. Bhavya[1]*, Raviraj Kusanur[2], D. Nagaraja[3], Vijaya Kumar[4] and N. L. Ramesh[4]

[1]Department of Physics, New Horizon College of Engineering, Bangalore - 560103, Karnataka, India; bhavyap26@gmail.com

[2]Department of Chemistry, R.V. College of Engineering, Bangalore - 560026, Karnataka, India

[3]Department of Physics, Bangalore Institute of Technology, Bangalore - 560004, Karnataka, India

[4]Department of Mathematics, M S Ramaiah Institute of Technology, Bangalore - 560054, Karnataka, India

Abstract

This study employs computational and experimental approaches to explore the spectral and photophysical features of the boronic acid derivative 2-Methoxy phenylboronic acid (2MEPBA). Various solvents exhibiting different levels of polarity and polarisability are employed to calculate the dipole moments in both the ground and excited states. With increasing solvent polarity, an increase in wavelength was seen, indicating a $\pi \rightarrow \pi^*$ transition caused by intermolecular charge transfer interactions. Additionally, experimentally measured dipole moment ($\Delta\mu$) values are compared to microscopic empirical solvent polarity (E_T^N) values. Density Functional Theory (DFT) calculations employing B3LYP/6-31+G (d, p) basis sets are utilised to explore molecular properties via quantum chemical simulations and conduct Frontier Molecular Orbital (FMO) analysis to study chemical reactivity and kinetic stability. The properties of Mulliken charges and Non-Linear Opticals (NLOs) are investigated further. Natural Bond Orbital (NBO) analysis reveals substantial stabilisation energy, indicating a specific donor-acceptor interaction via proton transfer. The software Schrodinger Maestro 11.2 was utilised to carry out docking studies. The binding affinities of 2MEPBA with periplasmic protein were determined using the GLIDE scores (PDB ID-2IPM). The spectroscopic and quantum computational work presented here is critical for using boronic acid derivatives as chemo sensors and the rational design of novel molecular probes. Boronic acid derivatives are in the early stages of development in the field of mining and efforts are being made to investigate the possible advantages of using them. Because of their special qualities, they could be useful instruments for raising safety, cutting costs, and increasing efficiency in the mining, minerals, and fuels sectors.

Keywords: Corrosion Inhibitors, DFT Studies, Dipole Moments, Fluorescence, Fuel Additives, Quantum Chemical Computations

1.0 Introduction

With the advance of modern science and technology, researchers have been able to examine the nature of life activities in greater depth thanks to fluorescent molecules for providing non-invasive, selective and sensitive research tools. The family of Boronic acids are one such fluorescent probes that are being explored as the active class of dyes known for their potential application in diverse fields of science and technology such as fluorescence imaging, chemo sensing[1], biomedical engineering, chemical biology[2], synthetic, organic chemistry[3], materials and

Author for correspondence

bioorganic chemistry[4,5]. Owing to the wide pharmaceutical and biochemistry applications, including the fields of mines, minerals and fuels, the spectroscopic investigations of these compounds have become a pressing need of the time. Also, derivatives of coumarins can be applied as corrosion inhibitors to shield metals from rust and other deterioration[6]. This is crucial since metals in the mining sector are subjected to hostile conditions.

Various fluorescent spectroscopic methods like solvatochromic method[7], rotational dynamic studies[8], quenching studies[9,10] and DFT studies[11] are some most commonly used techniques. Knowledge of dipole moments in their lower and higher energy states opens the window to understanding molecular geometry[12]. This is extremely useful when building new molecules for NLO applications[13]. DFT calculations present beneficial information on proximity reactivity descriptors by providing molecular reactivity and electron density data[14]. This facilitates the creation of novel pharmaceuticals and the comprehension of the interaction between material science and the biological system.[15].

Here, solvatochromic and DFT/B3LYP approaches are employed, respectively, to examine the dipole moments of 2MEPBA. The optimized molecular structure along with the integrated electronic density mapped with the Molecular Electrostatic Potential (MEP), NBO, FMO and NLO properties are all explored using the Gaussian 09 program. As these compounds can also be used in sensing applications, their interactions with amino acid residues of periplasmic proteins of the blood can also be studied by docking.

2.0 Materials and Methods

2.1 Materials

Laboratory synthesis was done for 2MEPBA using standard methods[16]. Figure 1 presents the structures of 2MEPBA. Solvents were procured from S-D-Fine Chemicals, India. Molecular docking studies for the sample were performed using the crystal structure of the galactose-binding periplasmic protein (PDB ID: 2IPM and 2IPL) which was obtained from the Protein Data Bank.

2.2 Dipole Moments Through Empirical Formula

The several solvatochromic equations that were used to calculate the dipole moments are credited to Bilot and Kawski, Lippert, Bakhshiev, Kawski-Chamma-Viallet and Reichardt[18-22]. Literature values from these papers were used for calculation.

2.3 Computation Using Quantum Chemistry

The 6-31+G (d, p) basis set via Gaussian 09 W[23] is used for the sample in the DFT/B3LYP approach for quantum chemical calculations. Theoretical dipole moments were computed in the gas phase. Using Gauss View 5.0 and gradient geometry optimization, the geometry of the compound was fully optimised[24]. NBO computation is done with NBO version 5.0[25].

3.0 Results and Discussion

3.1 Photophysical Behavior Analysis

3.1.1 Effects of Solvent on Spectra

The sample of 2MEPBA absorption spectra in 1, 4 dioxane is shown in Figure 2. The absorption spectra of 2MEPBA exhibit a peak of about 281-285nm with a shift in the maxima depending on the solvent utilised, as given in Table 1. The emission spectra as shown in Figure 3 show a single peak with a maximum of around 302-313nm for 2MEPBA with a solvent-dependent peak maximum shift. In comparison to emission spectra, absorption spectra show a smaller shift. Less significant absorbance shift with solvent polarity signifies less distortion in ground state energy distribution which is the fact for less polar molecule in ground state compared to its excited state. The substantial Stokes shift indicates that the higher state has a different geometry than the ground state. A molecule shows a standard solvatochromism with more sensitivity for polar solvents in its higher state. This is evident by the stoke shift changes. Further bathochromic shift with increasing solvent polarity in emission peak as seen in Table 1 affirms $\pi \rightarrow \pi^*$ transition.

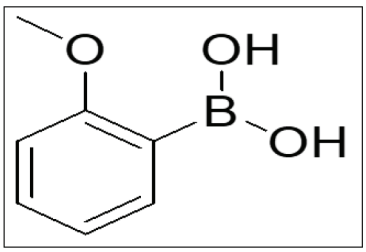


Figure 1. Molecular structure of MEPBA.

3.1.2 *Empirical Excited State Dipole Moments*

Table 2 sums up the different functions of different solvents. Band shift information from Table 1 was utilised to plot ($\bar{\nu}_a - \bar{\nu}_f$) v/s f(ε, n), ($\bar{\nu}_a + \bar{\nu}_f$) v/s φ(ε, n) charts with slopes m(1) and m(2) separately and are displayed from Figures 4(a) and 4(b). Plots of different functions are given in Figures 5, 6 and 7 with slopes m1, m2 and m3 respectively. Table 3 presents the data and analysis of the graphs which are further assessed utilising the following equations.

$$\mu_g = \frac{m^{(2)} - m^{(1)}}{2}\left[\frac{hca^3}{2m^{(1)}}\right]^{1/2} \quad (1)$$

$$\frac{\mu_e}{\mu_g} = \left[\frac{m^{(2)} + m^{(1)}}{m^{(2)} - m^{(1)}}\right] \quad (2)$$

$$\mu_g = \frac{m_3 - m_2}{2}\left[\frac{hca^3}{2m_2}\right]^{1/2} \quad (3)$$

$$\mu_e = \frac{m_3 + m_2}{2}\left[\frac{hca^3}{2m_2}\right]^{1/2} \quad (4)$$

and for $m_3 > m_2$

$$\mu_e = \left[\frac{m_2 + m_3}{m_3 - m_2}\right]\mu_g \quad (5)$$

Here molecular volume is used to determine "a". The above-calculated values are recorded in Table 4.

For unaligned dipole moments, then the angle between them φ can be determined by utilising Equation(6).

$$\cos\varphi = \frac{1}{2\mu_g\mu_e}\left[\left(\mu_g^2 + \mu_e^2\right) - \frac{m_3}{m_2}\left(\mu_e^2 - \mu_g^2\right)\right] \quad (6)$$

Equation (1) and Equation (2) are used to calculate the dipole minutes of the ground state and singlet excited energy states (2) where the ground state dipole moment is

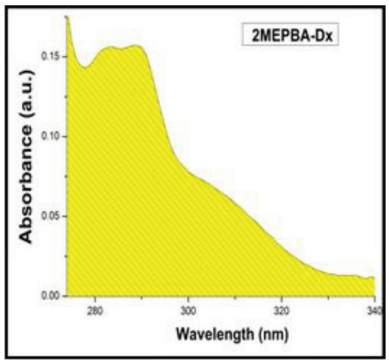


Figure 2. Typical absorption spectrum of 2MEPBA.

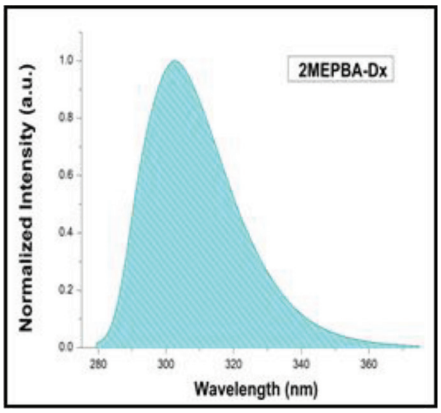


Figure 3. Typical emission spectrum of 2MEPBA.

Table 1. Photophysical parameters of 2MEPBA in different solvents

Solvent	λ_a (nm)	λ_f (nm)	$\bar{\nu}_a$ (cm^{-1})	$\bar{\nu}_f$ (cm^{-1})	($\bar{\nu}_a - \bar{\nu}_f$) ($cm^{-1}$)	($\bar{\nu}_a + \nu_f$) (cm^{-1})	½($\bar{\nu}_a + \bar{\nu}_f$) ($cm^{-1}$)
Heptane	281.5	302.0	35524.0	33112.6	2411.4	68637	34318.3
Cyclohexane	282.5	302.5	35398.2	33057.9	2340.4	68456	34228.0
1,4 Dioxane	282.0	302.0	35461.0	33112.6	2348.4	68574	34286.8
Toluene	284.5	305.0	35149.4	32786.9	2362.5	67936	33968.1
1 Butanol	284.0	310.5	35211.3	32206.1	3005.1	67417	33708.7
Ethanol	285.0	311.0	35087.7	32154.3	2933.4	67242	33621.0
Methanol	286.0	313.5	34965.0	31897.9	3067.1	66863	33431.5
Acetonitrile	286.0	311.5	34965.0	32102.7	2862.3	67068	33533.9
DMF	286.0	311.5	34965.0	32102.7	2862.3	67068	33533.9
DMSO	285.5	313.0	35026.3	31948.9	3077.4	66975	33487.6

around 1.11 D (μ_g^c) while the excited state dipole moment is 2.82D(μ_e^d). The angle formed by dipoles in their ground (μ_g^c) and excited energy state (μ_e^d) is determined by utilising Equation (6) to find if they are parallel to one another according to the suppositions in Bilot and Kawski conditions or if they form any angle.

As the angle between the dipole moments is zero, both electronic states are confirmed to be parallel to one another. Dipole moment increases on excitation recommended Intra-Atomic Charge (ICT) in excited energy state where the molecule turns more polar on excitation. μe value in Table 4 calculated from different methods show insignificant difference. Large excited state dipole moment values that determine distinct excited state geometry from the ground state were also anticipated by Lippert's method.

3.1.3 Solvent Polarity Parameter

Compared with the conventional approach of using the dielectric constant and refractive index of solvents in the form of functions, Reichardt's proposed empirical solvent parameter (E_T^N), which relates better with the spectral shift. Plots corresponding to (E_T^N) is shown in Figure 8 where the linear graph determines the general solute-solvent interactions. Slope 'm' of the above graph is used to calculate Δμ which is given by Equation (7).

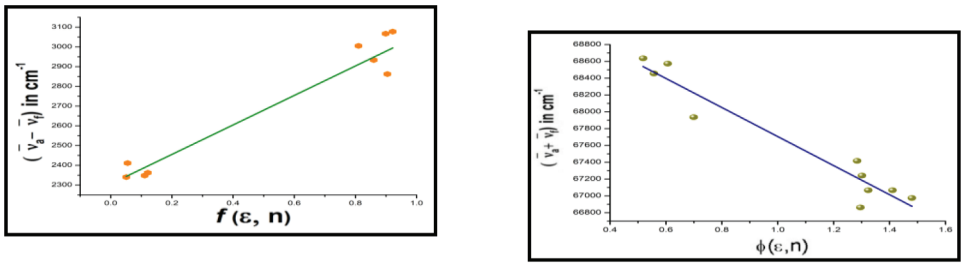
$$\Delta\mu = \left(\mu_e - \mu_g\right) = \sqrt{\frac{\text{mX81}}{\left(6.2/\text{a}\right)^3 11307.6}} \quad (7)$$

E_T^N values of all the solvents are referred from literature[22]. Utilising E_T^N, calculated excited state dipole moment as μ_e^i determined by Equation (7). Polarity changes with respect to the lower and higher energy states $\Delta\mu_e^j$ and $\Delta\mu_e^k$ are in Table 4. The observation of a decent agreement between the Reichardt and Bilot-Kawski approaches lends support to the higher excited state dipole moment. Additionally, the derivative of boronic acid exhibits a more polar nature in its excited energy state than in its ground state and has a higher change in dipole moment.

3.2 Quantum Computations

3.2.1 Optimised Structure

DFT/B3LYP/6-31+G(d,p) optimised geometry of the particle given in Figures 9 and 10 shows the gas phase



(A) **(B)**

Figure 4. Linear plots of 4(A) f(ε, n) and 4(B) φ(ε, n) of 2MEPBA using Bilot Kawaski.

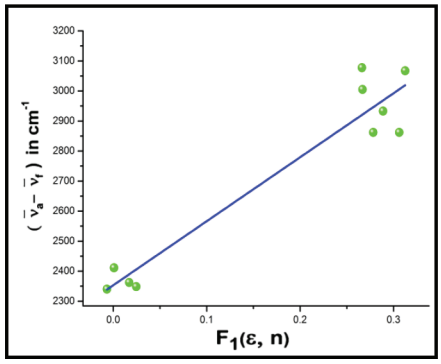


Figure 5. Linear plots of Stoke's shift v/s $F_1(\varepsilon, n)$

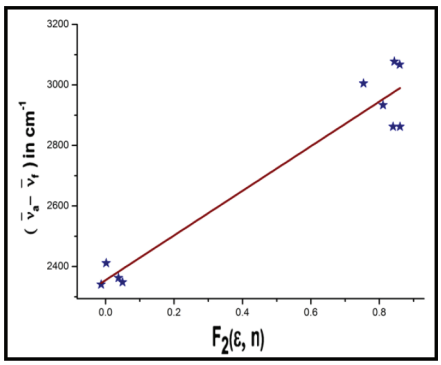


Figure 6. Linear plots of Stoke's shift v/s $F_2(\varepsilon, n)$.

DFT calculated ground state dipole moment with the value 3.17D. Noticed variation in theoretically determined dipole moment in comparison with experimental values is due to the way the theoretical computations are performed on an individual particle in the gaseous state.

3.2.2 *Frontier Molecular Orbital Analysis*

The energy gap created by the energy difference between Highest Occupied Molecular Orbital (HOMO) and Lowest Unoccupied Molecular Orbital (LUMO) plays a key role in describing the transport characteristics of

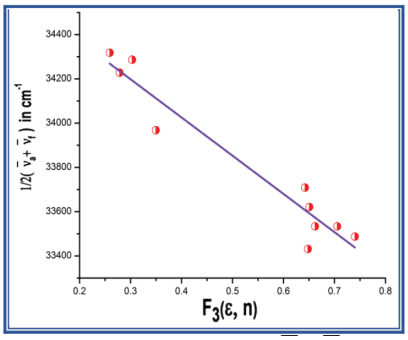


Figure 7. Linear plots of $1/2(\bar{\nu}_a+\bar{\nu}_f)$ v/s F_3 (ε, n)

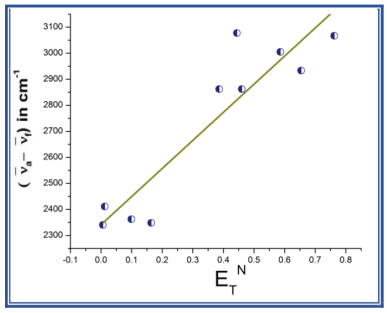


Figure 8. Linear plots of Stokes' shift v/s

Table 2: Dielectric constant (ε), refractive index (n), solvent polarity functions, microscopic solvent polarity parameters (E_T^N).

Solvent	ε	n	E_T^N	$F_1(\varepsilon,n)^a$	$F_2(\varepsilon,n)^b$	$F_3(\varepsilon,n)^c$	$\varphi(\varepsilon,n)^d$	$f(\varepsilon,n)^d$
1, 4 Dioxane	2.21	1.4	0.164	0.024682	0.049472	0.303191	0.606383	0.110858
Toluene	2.4	1.4	0.099	0.017104	0.037469	0.349645	0.69929	0.121057
1 Butanol	17.53	1.3	0.586	0.266778	0.753785	0.642037	1.284075	0.809977
Isopropanol	17.9	1.3	0.617	0.274776	0.763988	0.63376	1.26752	0.815148
1 Propanol	20.73	1.3	0.617	0.276601	0.783788	0.650358	1.300716	0.837444
Ethanol	24.13	1.3	0.654	0.288753	0.811143	0.650624	1.301247	0.859851
Methanol	33.61	1.3	0.762	0.312475	0.859689	0.647896	1.295792	0.899042
Acetonitrile	36.01	1.3	0.46	0.306170	0.860593	0.661876	1.323752	0.90453
DMF	37.31	1.4	0.386	0.278209	0.84033	0.705248	1.410496	0.904371
DMSO	47.13	1.4	0.444	0.266113	0.844059	0.739953	1.479905	0.921901

[Lippert]-Mataga solvent function
[b]Bakhshiev solvent function
[c]Kawski- Chamma- Viallet solvent function
[d]Bilot- Kawski polarity function

Table 3. Statistical treatment of the correlations of solvents spectral shifts of 2MEPBA.

Correlations	Slope		Correlation Factor "r"	Number of Data
Bilot- Kawaski Correlation	$m^{(1)}$	746.6	0.92	10
	$m^{(2)}$	1727.8	0.92	10
Lippert Correlation	m_1	2130.2	0.91	10
Bakhshiev's Correlation	m_2	737.2	0.92	10
Kawski-Chamma- Viallet's Correlation	m_3	1727.8	0.92	10
relation	m	1079.1	0.82	10

Table 4. Dipole moments of 2MEPBA.

Solute	Radius (A^0)	μ_g[a] (D)	μ_g[b] (D)	μ_g[c] (D)	μ_e[d] (D)	μ_e[e] (D)	μ_e[f] (D)	μ_e[g] (D)	μ_e[h] (D)	μ_e[i] (D)	$\Delta\mu$[j]	$\Delta\mu$[k]	ϕ[l]
2MEPBA	3.393	3.17	1.11	1.13	2.81	2.82	4.01	2.82	3.72	2.26	1.69	1.70	0°

[a]Dipole moment in the ground state calculated by Gaussian software.
[b]Dipole moment in the ground state calculated using the Bilot-Kawski method.
[c]Dipole moment in the excited state calculated using the Bilot-Kawski method.
[d]Dipole moment in the ground state calculated experimentally.
[e]Dipole moment in the excited state calculated experimentally.
[f]Excited state dipole moment calculated using the Lippert Mataga method.
[g]Excited state dipole moment calculated using the Bakhshiev method.
[h]Excited state dipole moment calculated using the Kawski-Charnma-Viallet method.
[i]Dipole moment calculated using the E^N_T equation of the Reichardt method.
[j]Change in dipole moments from the Bilot-Kawski method.
[k]Change in dipole moments calculated from E^N_T parameter.

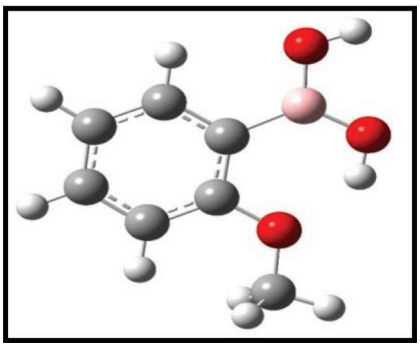


Figure 9. Optimised diagrams of 2MEPBA.

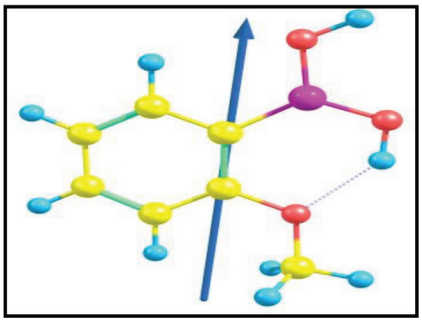


Figure 10. 2MEPBA's ground state-optimized molecular geometries. The direction of the dipole moment is indicated by the arrow.

the molecule. DFT/B3LYP is used to estimate frontier molecular orbitals. In Figure 11, the HOMO-LUMO 3D plots are presented. Here HOMO is localised on Phenyl and Methoxy group and LUMO is limited to Phenyl and Boronic acid group we can affirm that charge transfer occurs from the donor Methoxy group to the acceptor Boronic acid group.

The more stable the molecule will be if the energy gap is larger, and the molecule is more reactive if the energy gap is small. The following equations show different parameters[27,28], that are obtained using HOMO-LUMO values which helps in understanding the utility of molecules in different applications.

As per Koopmans' theorem we have[29]

Ionization potential (IP)-ELUMO

Electron affinity (EP)=EHOMO

Electronegativity (χ) =1/2 (IP+EA)

Chemical potential (μ)=1/2 (1P+EA)

Chemical hardness (η)=1/2 (1P-EA)

Chemical softness (S)= 1/ η

Electrophilicity (ω)= $\mu^2/2\eta$

Table 5 gives FMOs and the molecular property values calculated for 2MEPBA. The energy gap value for 2MEPBA is found to be 5.457 implying the molecule is more chemically stable. In our previous paper, we reported the studies of 2MEPBA (2-Methoxy-5-fluoro phenyl boronic acid)[11]. In comparison between 2MEPBA and 2MEFPBA, the un-substituted compound 2MEPBA has a higher energy gap and hence is less reactive and hard compared to Fluorine-substituted 2MEFPBA. The observed increased ionisation potential and lower electron affinities of 2MEPBA reveal the potential for nucleophilic and electrophilic attack.

3.2.3 MEP Analysis

MEPs represent electronic cloud surfaces which can be used to correspond to reactivity in a compound. The intensities of the electrostatic potential energy changes (for electrophilic and nucleophilic regions) are depicted

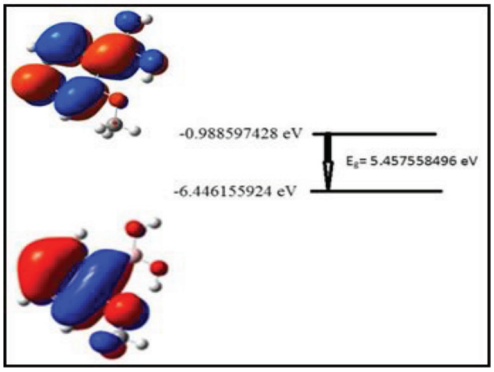


Figure 11. HOMO-LUMO structure of 2MEPBA.

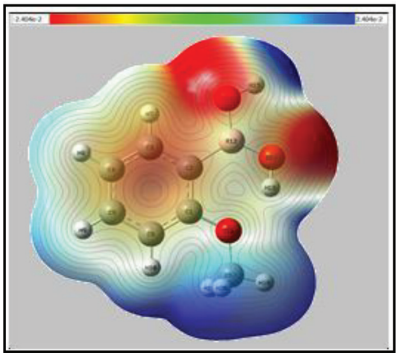


Figure 12. Electron density for 2MEPBA mapped using the MEP surface.

Table 5. FMO derived properties values of 2MEPBA

Molecule	IP	EA	P (eV)	χ(eV)	η (eV)	σ (eV)	ω (eV)
2MEPBA	6.466	0.988	-3.717	3.717	2.729	0.366	1.850

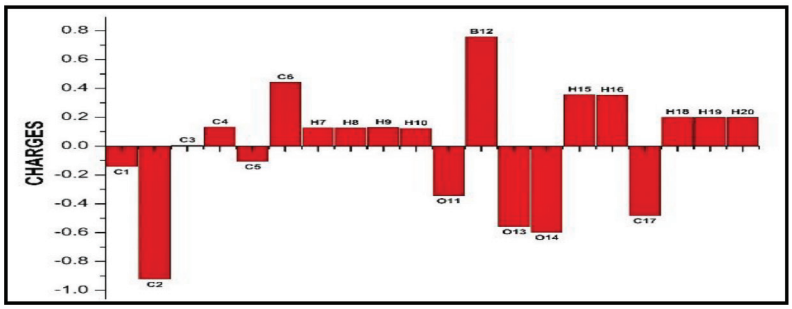


Figure 13. Mulliken charges for 2MEPBA.

using red and blue colour codes as the lowest and highest electrostatic potential energy value[29].

The calculated value of MEP and optimised geometry for the compound are mapped and shown in Figure 12. Around the hydrogen atom of both the boronic group and the methoxy group, nucleophilic behaviour is seen as it has a deep dark blue region and electrophilic nature is observed for Boronic group oxygen atoms with a deep red colour. MEP and contour analysis together display the nucleophilic and electrophilic reaction sites. The contour map on MEP further supports positive and negative regions as depicted by the total electron density surface which is shown in Figure 12.

3.2.4 Mulliken Atomic Charges

Mulliken investigations are used to compute atomic charge analysis and define charge transfer, which determines the molecular reactivity of the compound. For this investigation, 6-31+G (d, p) basis level B3LYP techniques are employed where Figure 13 shows the Boronic acid derivative Mulliken charge distribution. Here the observation shows that O atoms have a negative charge, while Boron and all H atoms have a positive charge. Both positive and negative charges are observed for C atoms as in Figure 13 and are highly influenced by their substituents and act as a centre for charge transfer in Boronic acid. For a total of 20 atoms, the 6th position carbon atom to which the Boronic acid group is attached in the phenyl ring has a maximum negative charge. This shows that the centre of charge transfer between the substituents and the phenyl ring is the carbon atoms linked to the phenyl ring that have the highest negative charges.

3.2.5 NLO

NLO properties finding major applications are correlated with molecular structures[30] with polarisability and hyperpolarisability computation where large

hyperpolarisabilities are preferred. α, μ and β_{ijk} were calculated using DFT/B3LYP with 6-31+G (d, p) basis level for the compound.

Calculated values of Polarisabilities and hyperpolarisabilities are found to be 15.6784 and $0.4898X10^{-30}$ for 2MEPBA in esu units and are tabulated in Table 6. Computed values of dipole moment for 2MEPBA are compared with prototypical urea and is found that the value is 0.814 times of urea. For 2MEPBA, it is discovered that hyperpolarisabilities are 0.7877 times higher than urea (tot = 0.6218 X 10^{-30} esu). This indicates that the study helps to explore in detail, the NLO properties and also helps in the design of newer molecules.

3.2.6 NBO Analysis.

Intra and intermolecular bonding explanation, analysis of stability, transfer of charge and conjugative interaction are analysed by NBO analysis tool[31] from Gaussian 9W software. A perturbative calculation leads to bonding and anti-bonding interactions, which are estimated by the NBO method. This method expresses stabilisation energy linked with the delocalization value of i, j as an estimate of Lewis and Non-Lewis type interactions owing to second-order perturbation theory[32].

The bonding and anti-bonding efficient interactions are calculated and listed in Table 7. As observed from the table we have two types of donors and acceptors pairs (σ, π, σ* and π*) and depict the following most probable transitions with the understanding of perturbation energy E2. For 2MEPBA hyper-conjugative interactions are of second-order type taking place between lone pairs and σ orbitals or between σ and σ* orbitals and are only found within the Phenyl ring. We have transitions as; C(1-2) → C (3-4), C(1-2) →C(5-6, C(3-4) to C(1-2) and C(5-C6) all attributing π→π* transition. They are centred on the carbon atoms to which substitutions are attached on the ring. The orbital overlap between the σ(C–H) and σ*(C–H) bond orbitals in methoxy groups, such as C17-H18 and C17-H18, has shown strong intramolecular interactions in boronic acid derivatives.

Table 6. NLO properties of 2MEPBA.

	a.u	esu(x10^{-24})		a.u	esu(x10^{-33})
α_{xx}	128.1231	18.9878	β_{xxx}	134.1280	1158.772
α_{xy}	-0.0018	-0.0007	β_{yxx}	0.0316	0.2730
α_{yy}	63.8975	9.4691	β_{xyy}	79.1864	684.1151
α_{xz}	0.2658	0.0393	β_{yyy}	0.0834	0.7205
α_{yz}	-0.0047	-0.0007	β_{zxx}	176.6961	1526.531
α_{zz}	125.3562	18.5777	β_{xyz}	0.03569	0.3083
α_{0}	105.7923	15.6784	β_{zyy}	-25.4065	-219.494
Δα	62.8895	9.3202	β_{xzz}	6.9490	60.0345
μ_{x}	0.1000		β_{yzz}	-0.0030	-0.0259
μ_{y}	0.0005		β_{zzz}	-75.6635	-653.68
μ_{z}	-1.2462		β_{0}	56.6956	489.8
μ	1.2502	3.1771 Debye			

3.2.7 Molecular Docking Studies

Using VMD 1.9.3, docking preparation and pre-processing were carried out and the protein data bank was consulted to obtain the crystal structures of the periplasmic proteins that bind galactose (PDB IDs: 2IPM and 2IPL).

To perform the molecular docking for 2MEPBA, the 1.5.6 version of Auto Dock Tools software was used as shown in Figures 14 and 15. The docking energy profile and interactions with amino acid residues are shown in Table 8.

Table 7. Bonding and antibonding analysis of 2MEPBA.

Donor(i)	E_D(e)	Accepter(j)	E_D(e)	$E_{(2)}$kcal/mol	E_j-E_i (a.u.)	$F_{(I,j)}$ (a.u.)
π (C1-C2)	1.63886	π*(C3-C4)	0.32915	19.85	0.28	0.065
π (C1-C2)	1.63886	π*(C5-C6)	0.33488	20.02	0.28	0.067
π (C3-C4)	1.65894	π*(C1-C2)	0.36302	20.87	0.28	0.069
π (C3-C4)	1.65894	π*(C5-C6)	0.33488	20.68	0.27	0.067
π (C5-C6)	1.66926	π*(C1-C2)	0.36302	20.17	0.28	0.068
π (C5-C6)	1.66926	π*(C3-C4)	0.32915	19.23	0.28	0.065
σ (C17-H18)	1.79152	σ*(C17-H18)	0.08467	9.44	0.86	0.083
σ (C17-H19)	1.74598	σ*(C17-H18)	0.08467	7.43	0.97	0.079

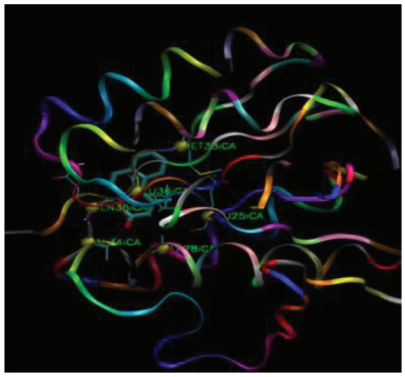


Figure 14. Best affinity mode of docked 2MEPBA with 2-IPM protein.

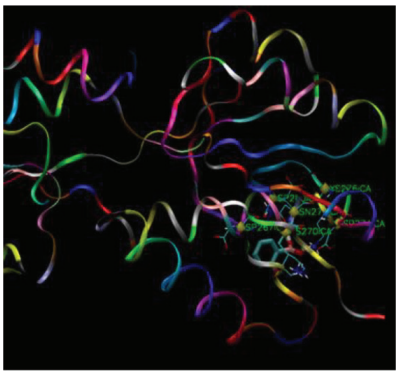


Figure 15. Best affinity mode of docked 2MEPBA with 2-IPL protein.

Table 8. Interaction of 2IPM and 2IPL protein for 2MEPBA with docked energy parameters.

Docked Energy Parameters	2IPM	2IPL
Binding_Energy (kcal/mol)	-5.97	-5.98
Ligand_Efficiency	-0.54	-0.54
Inhib_Constant	42.42 (uM)	41.67 (uM)
Intermol_Energy (kcal/mol)	-7.16	-7.17
Electrostatic energy (kcal/mol)	-2.15	-2.72
Total_Internal Energy. (kcal/mol)	0.14	-0.35
Torsional_Energy. (kcal/mol)	1.19	1.19
Unbound_Energy (kcal/mol)	0.14	-0.35
Hydrogen Bonds	LYS276, LYS285 LYS22, ARG21	LYS113, LYS58
Interaction with Amino acids within 3.5 A° of Ligand	ASP111, SER112, LYS113, ALA157, TYR161	ASP267, LYS270, ASN271, ASP274, LYS276, ASP280

4.0 Conclusions

The following interpretations are derived from the above discussion, for the studied heterocyclic compound 2MEPBA where fluorescence spectroscopic behaviour and quantum computations are carried out.

(1) From all types of solvatochromic approaches dipole moment calculated for the test molecule is greater in the excited energy state than in the ground state. Although dipole moments are found to be less Δμ variation is very prominent. This illustrates boronic acid derivatives to have large charge distribution and more polar nature in excited state than in ground states.

(2) An increase in the polarity of the solvent causes a red shift in the Stokes line. This confirms $\pi \rightarrow \pi^*$ the transition for both the molecules together with the ICT character.

(3) The DFT-based phase optimises the diagram and the direction of the ground state dipole moment is obtained. The stable six-membered chelate formed the dye highly stable.

(4) Local and global parameters are analysed from FMO analysis which show that Boronic acid derivate has good chemical stability and strength

(5) The NLO properties of test molecules are analysed by comparing their first hyperpolarisabilities with those of the prototypical NLO materials and confirm Boronic acid derivative is less active.

(6) The docking study revealed that at active sites, the compound 2MEPBA showed the best suitable binding pattern by interacting non-covalently with amino acid residues of the proteins.

Substituted heterocycles present a wide range of diversity and hold crucial applications. Thus, it is crucial to look at the many photophysical characteristics of these more recent molecules as well as how they interact with other substances. Specific applications of boronic acid derivatives in the fields of mines and minerals would depend on their chemical properties, stability under relevant conditions, and their effectiveness in achieving the desired outcomes. Additionally, ongoing research may

lead to the discovery of new applications or derivatives with improved performance. Therefore, this work addresses some of the important photophysical features in addition to quantum chemical structure analysis, which will further expand the body of knowledge to investigate newer molecules.

5.0 Acknowledgements

The authors are thankful for the grant (GRD no: 1106/2021-22/ 491) from the Department of Science and Technology (DST), Government of India and Vision Group of Science and Technology (VGST), Government of Karnataka which helped in setting up a computational workstation.

6.0 References

1. Boyet M, Chabaud L, Pucheault M. Recent advances in the synthesis of Borinic acid derivatives. Molecules. 2023; 28(6):2660. https://doi.org/10.3390/molecules28062660 PMid:36985634 PMCid: PMC10057197.
2. Escada-Rebelo S, Mora FG, Sousa AP, Almeida-Santos T, Paiva A, Ramalho-Santos J. Fluorescent probes for the detection of reactive oxygen species in human spermatozoa. Asian J Androl. 2020; 22(5):465. https://doi.org/10.4103/aja.aja_132_19 PMid:31939350 PMCid: PMC7523605.
3. Zeng X, Chen X, Chen J, Ma M, Jin H, Yu S, Liu Z. A simple highly selective ratiometric fluorescent probe for detection of peroxynitrite and its bioimaging applications. Dyes Pigm. 2023; 210:110993. https://doi.org/10.1016/j.dyepig.2022.110993
4. Bassan E, Gualandi A, Cozzi PG, Ceroni P. Design of BODIPY dyes as triplet photosensitizers: electronic properties tailored for solar energy conversion, photoredox catalysis and photodynamic therapy. Chem Sci. 2021; 12(19):6607-28. https://doi.org/10.1039/D1SC00732G PMid:34040736 PMCid: PMC8132938.
5. Papadopoulos J, Mueller TJ. Rapid synthesis of 4-alkynyl coumarins and tunable electronic properties of emission solvatochromic fluorophores. Dyes Pigm. 2019; 166:357-66. https://doi.org/10.1016/j.dyepig.2019.03.038
6. Elaryian HM, Bedair MA, Bedair AH, Aboushahba RM, Fouda AE. Synthesis, characterization of novel coumarin dyes as corrosion inhibitors for mild steel in acidic environment: Experimental, theoretical and biological studies. J Mol Liq. 2022; 346:118310. https://doi.org/10.1016/j.molliq.2021.118310
7. Kajiwara K, Osaki H, Greßies S, Kuwata K, Kim JH, Gensch T, Sato Y, Glorius F, Yamaguchi S, Taki M. A negative-solvatochromic fluorescent probe for visualizing intracellular distributions of fatty acid metabolites. Nat Commun. 2022; 13(1):2533. https://doi.org/10.1038/s41467-022-30153-6 PMid:35534485 PMCid:PMC9085894.
8. Howe ME, Garcia-Garibay MA. Fluorescence and rotational dynamics of a crystalline molecular rotor featuring an aggregation-induced emission fluorophore. J Org Chem. 2019; 84(15):9570-6. https://doi.org/10.1021/acs.joc.9b01201 PMid:31288516.
9. Sharma K, Melavanki R, Muttannavar VT, Bhavya P, Meghana U, Suma B. Fluorescence spectroscopic studies on preferential solvation and bimolecular quenching reactions of Quinolin-8-ol in binary solvent mixtures. In J Phys Conf Ser. 2020; 1473: 1:012045. IOP Publishing. https://doi.org/10.1088/1742-6596/1473/1/012045
10. Bhavya P, Melavanki R, Kusanur R, Sharma K, Muttannavar VT, Naik LR. Effect of viscosity and dielectric constant variation on fractional fluorescence quenching analysis of coumarin dye in binary solvent mixtures. J Lumin. 2018; 33(5):933-40. https://doi.org/10.1002/bio.3492 PMid:29745063
11. Bhavya P, Melavanki R, Sharma K, Kusanur R, Patil NR, Thipperudrappa J. Exploring the spectral features and quantum chemical computations of a novel biologically active heterocyclic class of compound 2MEFPBA dye: Experimental and theoretical approach. Chem Data Collect. 2019; 19:100182. https://doi.org/10.1016/j.cdc.2019.100182
12. Muddapur GV, Melavanki R, Sharma K, Srinivasa HT, Thipperudrappa J, Patil NR. Fluorescence properties of aromatic asymmetric di-ketone compound in polar and non-polar solvents. In J Phys: Conf Ser 2020; 1473(1):012044. IOP Publishing. https://doi.org/10.1088/1742-6596/1473/1/012044
13. Zaitri KL, Mekelleche SM. Computational study of linear and nonlinear optical properties of substituted thiophene imino dyes using long-range corrected hybrid DFT methods. Mol Phys. 2020; 118(4):1618508. https://doi.org/10.1080/00268976.2019.1618508
14. Frau J, Glossman-Mitnik D. Conceptual DFT study of the local chemical reactivity of the dilysyldipyrrolones A and B intermediate melanoidins. Theor Chem Acc. 2018; 137(5):67. https://doi.org/10.1007/s00214-018-2244-x
15. Flores-Holguín N, Frau J, Glossman-Mitnik D. Computational chemistry and molecular modelling techniques for the study of Micropeptin EI-964: Insights into its chemical reactivity and potential pharmaceutical properties. Comput Mol Biosci. 2023; 13(3):35-47. https://doi.org/10.4236/cmb.2023.133003
16. Kusanur RA, Kulkarni MV. A novel route for the synthesis of Recemic 4-(Coumaryl) Alanines and their antimicrobial activity. Asian J Chem. 2014; 26(4):1077. https://doi.org/10.14233/ajchem.2014.15865

17. Sharma K, Melavanki R, Yallur BC, Kusanur R, Patil NR, Shelar VM, Singh D, Rosario J, Hussaini Q, Thampan AV. Optical characterization of chalcone-doped PMMA thin films for photonic applications using spectroscopic technique of drop casting method. In Macromol Symp. 2020; 392(1):2000165. https://doi.org/10.1002/masy.202000165
18. Bilot L, Kawski A. Zur theorie des einflusses von lösungsmitteln auf die elektronenspektren der moleküle. Z Naturforsch A. 1962; 17(7):621-7. https://doi.org/10.1515/zna-1962-0713
19. Bilot L, Kawski A. Dipolmomente einiger phthalimid-derivate im ersten angeregten singulettzustand. Z Naturforsch A. 1963; 18(2):256-6. https://doi.org/10.1515/zna-1963-0228
20. Lippert E. Spectroscopic determination of the dipole moment of aromatic compounds in the first excited singlet state. Z Elektrochem. 1957; 61(8):962-75. https://doi.org/10.1002/bbpc.19570610819
21. Bakhshiev NG. Universal intermolecular interactions and their effect on the position of the electronic spectra of molecules in 2-component solutions. 7. Theory (general case for isotopic solution). Opt Spektroskopiya. 1964; 16(5):821-32.
22. Reichardt C. Solvatochromic dyes as solvent polarity indicators. Chem Rev. 1994; 94(8):2319-58. https://doi.org/10.1021/cr00032a005
23. Melavanki R, Sharma K, Muttannavar VT, Kusanur R, Katagi K, Patra SM, Umapathy S, Sadasivuni KK, Shelar VM, Singh D, Patil NR. Quantum chemical computations, fluorescence spectral features and molecular docking of two biologically active heterocyclic class of compounds. J Photochem Photobiol A. 2021; 404:112956. https://doi.org/10.1016/j.jphotochem.2020.112956
24. Dennington R, Keith T, Millam J, Eppinnett K, Hovell WL, Gilliland R. GaussView, Version 3.09, Semichem. Inc., Shawnee Mission, KS. 2003; 2(1). https://scholar.google.co.in/scholar?hl=en&as_sdt=0%2C5&q=Dennington+et+al.%2C+2003&btn
25. Glendening ED, Weinhold F. Natural resonance theory: II. Natural bond order and valency. J Comput Chem. 1998; 19(6):610-27. https://doi.org/10.1002/(SICI)1096-987X(19980430)19:6<610::AID-JCC4>3.0.CO;2-U
26. Muddapur GV, Melavanki RM, Patil PG, Nagaraja D, Patil NR. Photophysical properties of 3MPBA: Evaluation and co-relation between solvatochromism and quantum yield in different solvents. J Mol Liq. 2016; 224:201-10. https://doi.org/10.1016/j.molliq.2016.09.102
27. Atilgan AB, Yurdakul ŞE, Erdogdu Y, Güllüoğlu MT. DFT simulation, quantum chemical electronic structure, spectroscopic and structure-activity investigations of 4-acetylpyridine. J Mol Struct. 2018; 1161:55-65. https://doi.org/10.1016/j.molstruc.2018.01.080
28. Mohan B, Choudhary M, Bharti S, Jana A, Das N, Muhammad S, Al-Sehemi AG, Kumar S. Syntheses, characterizations, crystal structures and efficient NLO applications of new organic compounds bearing 2-methoxy-4-nitrobenzeneamine moiety and copper (II) complex of (E)-N'-(3, 5-dichloro-2-hydroxybenzylidene) benzohydrazide. J Mole Struct. 2019; 1190:54-67. Rubio-Pons Ò, Luo Y, Ågren H. Effects of conjugation length, electron donor and acceptor strengths on two-photon absorption cross sections of asymmetric zinc-porphyrin derivatives. J Chem Phys. 2006; 124(9). https://doi.org/10.1016/j.molstruc.2019.04.059
29. Lakshminarayanan S, Jeyasingh V, Murugesan K, Selvapalam N, Dass G. Molecular electrostatic potential (MEP) surface analysis of chemo sensors: An extra supporting hand for strength, selectivity & non-traditional interactions. J Photochem Photobiol. 2021; 6:100022. https://doi.org/10.1016/j.jpap.2021.100022
30. George M, Balaji J, Sajan D, Dominic P, Philip R, Vinitha G. Synthesis and third-order optical nonlinearity studies of toluidine tartrate single crystal supported by photophysical characterization and vibrational spectral analysis. J Photochem Photobiol. A: Chemistry. 2020; 393:112413. https://doi.org/10.1016/j.jphotochem.2020.112413
31. Frisch A. Gaussian 09W Reference. Wallingford, USA, 25p. 2009;470. https://www.chemistry4.me/Gaussian/G09W/help/g09w_ref.pdf
32. Yeliz UL. Natural bond orbital (NBO) population analysis and non-linear optical (NLO) properties of 2-(azepan-1-yl (naphthalen-1-yl) methyl) phenol. Int J Chem Technol. 2020; 4(2):138-45. https://doi.org/10.32571/ijct.751001